Computational Materials Science 93 (2014) 151–159

Contents lists available at ScienceDirect

Computational Materials Science

journal homepage: www.elsevier.com/locate/commatsci

Theoretical investigation of band gap and optical properties of $ZnO_{1-x}Te_x$ alloys (x = 0, 0.25, 0.5, 0.75 and 1)

N.A. Noor [a], S. Ali [a], G. Murtaza [b], M. Sajjad [c], S.M. Alay-e-Abbas [d,e], A. Shaukat [e], Z.A. Alahmed [f], A.H. Reshak [g,h,*]

[a] Department of Physics, University of the Punjab, Quaid-e-Azam Campus, Lahore 54590, Pakistan
[b] Centre for Advanced Studies in Physics, G.C. University, Lahore 54000, Pakistan
[c] School of Electronic Engineering, Beijing University of Posts and Telecommunications, Beijing 100876, China
[d] Department of Physics, GC University Faisalabad, Allama Iqbal Road, Faisalabad 38000, Pakistan
[e] Department of Physics, University of Sargodha, Sargodha 40100, Pakistan
[f] Department of Physics and Astronomy, King Saud University, Riyadh 11451, Saudi Arabia
[g] New Technologies – Research Center, University of West Bohemia, Univerzitni 8, 614 Pilsen, Czech Republic
[h] Center of Excellence Geopolymer and Green Technology, School of Material Engineering, University Malaysia Perlis, 01007 Kangar, Perlis, Malaysia

ARTICLE INFO

Article history:
Received 22 March 2014
Received in revised form 27 May 2014
Accepted 13 June 2014

Keywords:
Special quasi-random structure
Rock-salt (RS)
Zinc-blende (ZB)
$ZnO_{1-x}Te_x$ alloys

ABSTRACT

In this study, the special quasi-random structure (SQS) approach has been considered for structural, electronic and optical properties of rock-salt (RS) and zinc-blende (ZB) phases of $ZnO_{1-x}Te_x$ (x = 0, 0.25, 0.5, 0.75 and 1) using density functional theory. The Wu–Cohen generalized gradient approximation (GGA) has been employed for optimizing the lattice parameters (a_0) and bulk moduli (B_0) in both phases which show reasonable agreement with numerous theoretical and experimental results. To compute the band gaps with high degree of precision, we employed Engel–Vosko GGA and modified Becke and Johnson local density approximation (mBJLDA) functionals. In the RS phase, metallic nature of the compounds under investigation is evident for $0.25 < x < 1$, whereas direct band gap appears at all concentrations in ZB phase. The density of states (total and partial) are presented to comprehensively analyze the electronic structure of all compounds. Contrary to earlier theoretical studies, the mBJLDA band gap values for the end binaries appear to be significantly improved showing overall better agreement with the experimental data. The optical properties of $ZnO_{1-x}Te_x$ alloys in the ZB phase are also discussed in terms of dielectric function which show their potential utilization in optoelectronic devices.

1. Introduction

The high complexity of pristine and defective forms of II–VI wide-gap semiconductors has made these materials one of the hot topics in the current condensed matter research [1–6]. Among these semiconductors, ZnO stands out for future technological needs due to its suitability for various electronic, optical and magnetic devices which has been the reason behind numerous experimental and theoretical investigations for this material [1,7]. The increasing interest in ZnO originated from its promising applications in spintronic and opto-electronic devices. Moreover, ZnO is already being used in applications which range from fabrication of solar cells, light emitting diodes (LEDs), ultraviolet (UV) opto-detectors to piezo-electronic devices and thin film transistors [1,2,8–11]. In addition, the attractive properties of ZnO nanocrystals, such as hysteresis above ambient, lasing ability in ultraviolet and visible region at room temperature as well as selective sensing of glasses are well understood and already playing a crucial technological role [12–14]. The possibility to grow large size ZnO crystal and wafer by modern techniques has struck an immediate chord with researchers interested in its industrial use [15]. Substantial progress has been made in understanding this material and remarkable new properties of polycrystalline and nanocrystalline ZnO are discovered which are very important from technological point of view [5,8,12,16–20].

On the other hand, II–VI wide-gap semiconductors ZnTe has attracted a great deal of attention being a natural candidate for opto-electronic device applications like detectors, light emitting diodes (LEDs) and window material for CdTe based solar cells [21–23]. Various fabrications techniques such as molecular beam epitaxy (MBE), thermal vacuum evaporation (TVE), vapor phase deposition (VPD) and electrochemical deposition have

* Corresponding author at: New Technologies – Research Center, University of West Bohemia, Univerzitni 8, 6 14 Pilsen, Czech Republic. Tel./fax: +420 777729583.
E-mail address: maalidph@yahoo.co.uk (A.H. Reshak).

http://dx.doi.org/10.1016/j.commatsci.2014.06.017
0927-0256/

been successfully employed for the growth of ZnTe thin films [24–27].

Although a large number of theoretical and experimental studies are available on anion-substituted alloys such as ZnO_xS_{1-x} [28], a comprehensive account of ground state properties of $ZnO_{1-x}Te_x$ alloys in cubic rocksalt (RS) and zincblende (ZB) phases in not available in literature, to the best of our knowledge. In the present study we utilize density functional theory (DFT) to explore some opto-electronic properties of $ZnO_{1-x}Te_x$ alloys in order to identify their utilization in future devices.

2. Computational details

The correlations of random alloys in periodic structures do not remain accurate after a certain lapse of distance. A simple solution to this problem demands the construction of large supercell, however, first-principles calculations become increasingly expensive with increasing number of atoms in the supercell. Based on the fact that physical properties which depend on local randomness and microscopic length are not affected by the size of supercell, Zunger et al. [29] proposed construction of special quasirandom structure (SQS) supercells with the advantage of leaving their size on the choice of user. In the present study a limiting case of infinitesimal supercells compatible with the constituents in percentage is therefore used. Consequently, the $ZnO_{1-x}Te_x$ compounds are schemed in terms of periodically repeated supercells with preferred compositions in ordered structure. By using the compositions $x = 0.25$, 0.5 and 0.75, we considered eight-atom cubic lattice for exploring the physical properties of $ZnO_{1-x}Te_x$ alloy in RS and ZB phase. For constructing a SQS, it is required to closely reproduce the structural correlation function of the random alloy for first few neighboring shells and, therefore, the characterization of SQS depends upon this correlation functions (detailed analysis can be found in Ref. [29]). In the present study, the structures used for mimicking the random alloy at $x = 0.25/0.75$ and $x = 050$ belong to the eight atom SQS [29]. For the case of $x = 0.25$ and 0.75, the simplest structure is a simple cubic lattice with eight atom. For the case of ZB alloys, this structure has the anions with lowest concentration at the simple cubic lattice site which is usually termed as the luzonite structure. On the other hand, the structure obtained for the case of $x = 0.50$ is simply a (001) supercell. Similar first-principles SQSs have been successfully applied to binary and ternary solid solutions for accurate prediction of various properties of solid solutions [30]. The basic advantage of SQS approach is that it helps overcome limitations when studying various physical properties of disordered solid solutions by allowing for substitution of atoms at lattice sites such that the resulting structures reproduce the average correlation functions of the random substitutional alloys. In spite of the fact the eight atom SQS is generally too small to represent a random alloy, our calculated results for fundamental band gap indicate that for the case of $ZnO_{1-x}Te_x$ an eight-atom and a thirty two-atom structure show very little differences. Therefore, for the results presented in subsequent sections we utilize the smallest SQS (Fig. 1) which effectively reduce the calculation times.

Full-potential linear-augmented-plane-wave plus local-orbital (FP-LAPW + lo) method of DFT, as implemented in the WIEN2K package [31], has been used in this study to compute the electronic structure and optical properties of $ZnO_{1-x}Te_x$ alloys in RS and ZB phase. The self-consistent field energy tolerance is set to 10^{-4} Ryd and the electronic exchange–correlation for structural optimization is managed by generalized gradient approximation (WC-GGA) [32]. The reason for utilizing WC-GGA for structural optimization stems from its better performance for geometry optimization as compared to other DFT parameterizations schemes [33]. In order to improve the usual underestimation of band gaps by standard DFT functionals, the Engel and Vosko GGA [34] and the modified Becke–Johnson local density approximation (mBJLDA) [35] functionals have been employed to compute electronic and optical properties.

In the FP-LAPW + lo calculations. the wave function and potentials in the interstitial regions were expanded in terms of spherical harmonic and a plane wave with cutoff $K_{max} * R_{MT} = 8$ is used for the convergence of energy eigenvalues. Here, R_{MT} is the smallest of the muffin-tin (MT) sphere radius and K_{max} is the magnitude of largest K vector in plane wave expansion. The selected radius of MT sphere (R_{MT}) are 2.05 a.u., 2.3 a.u. and 1.80 a.u. for Zn, Te and O, respectively. The maximum value of angular momentum ($l_{max} = 10$) is taken for the wave function expansion within the atomic spheres. While, charge density was Fourier expanded up to $G_{max} = 18$, where G_{max} is the largest vector in the Fourier

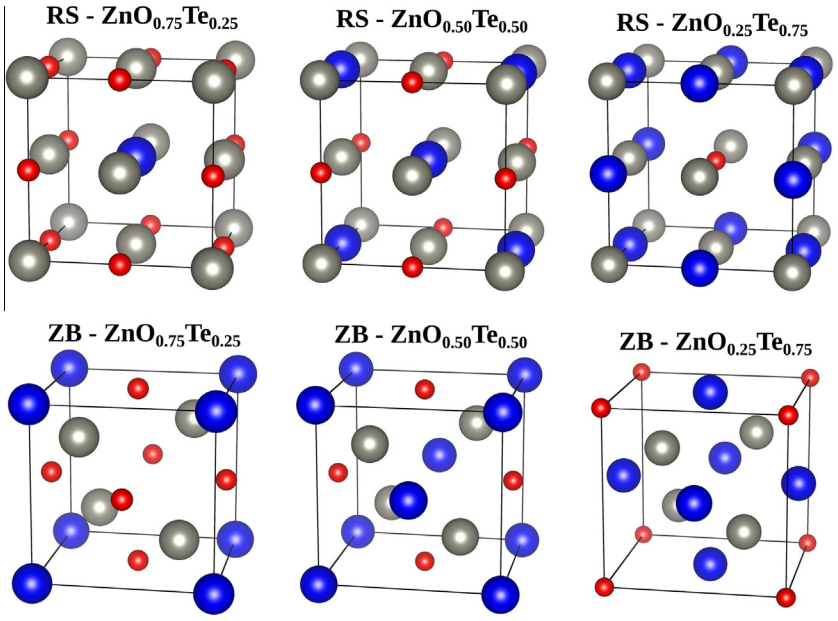

Fig. 1. Special quasi-random structure (SQS) for $ZnO_{1-x}Te_x$ at $x = 0.25$, 0.50 and 0.75 in (a) RS and (b) ZB phase.

expansion. For energy calculations, the Brillouin zone integration has been affected with $12 \times 12 \times 12$ k-mesh for the compounds in the irreducible part of the Brillouin zone. In order to achieve good convergence, both the MT radius and the number of k-points are varied by selecting the values which yield true convergence of minimum total energy.

3. Results and discussion

3.1. Structural properties

The structural properties of modeled RS and ZB alloys along with their end binaries are computed using the WC-GGA. Similar to the procedure adopted in recent theoretical studies [36–38], we use the SQS approach to obtain alloy supercell in the RS and ZB phase by repeating a unit cell of eight atoms in three dimensions. For the $ZnO_{1-x}Te_x$ ($x = 0.25$, 0.50 and 0.75) and the end binary compounds, the total energy has been estimated in terms of unit cell volume as shown in Fig. 2. At each concentration, the optimized ground state lattice parameter and bulk modulus are provided in Tables 1 and 2. Our computed values for ZnO and ZnTe (in both RS and ZB phases) have excellent agreement with experiment and most recent theoretical studies which is due to the fact that WC-GGA yields structural parameters which are in between the overestimated and underestimated results of market standard GGA and LDA functionals, respectively. The computed lattice parameters of the alloys in both phases are linearly increasing with the increasing dopant concentration. In Fig. 3(a), the variation of lattice parameter with x compared with the Vegard's law [39]. Referring to Fig. 3(a), one can appreciate the DFT calculations by finding a significant deviation of our results from the Vegard's law. On the other hand, the bulk modulus linearly decreases (Fig. 3(b)) with the increasing x concentration showing that the compounds under study become more compressible. One reason behind the deviations observed in Figs. 3 from Vegard's law is a consequence of the mismatch in bulk modulus and lattice parameter of ZnO and ZnTe compounds. In addition to that, the calculated structural parameters deviate from experimental due to the fact that exchange–correlation functionals of DFT attempt to map a interacting system (exact solution) on to a non-interacting system (approximate solution) through numerical approximation. This approximate nature of DFT together with the parametric mismatch

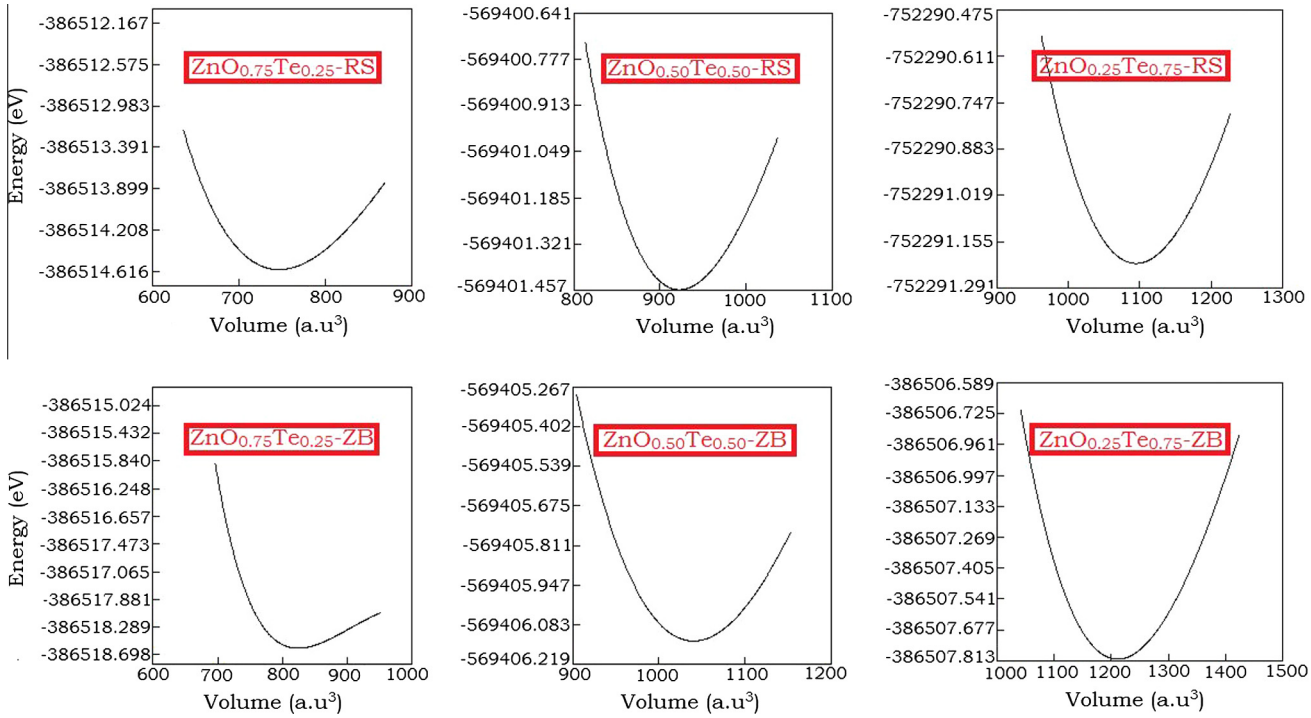

Fig. 2. Calculated total energy as a function of unit cell volume for $ZnO_{1-x}Te_x$ alloys at $x = 0.25$, 0.50 and 0.75 in RS and ZB phases.

Table 1
Calculated rock-salt (RS) phase structural parameters for $ZnO_{1-x}Te_x$ alloys compared with experimental and other theoretical calculations.

Composition	Lattice constant a (Å)			Bulk modulus B (GPa)		
X	WC-GGA	Other calculations	Exp.	WC-GGA	Other calculations	Exp.
0	4.26	4.225[b], 4.294[c]	4.28[a]	200.29	209.1[b], 203.3[c]	228[a]
0.25	4.80			125.92		
0.50	5.15			89.27		
0.75	5.45			72.01		
1	5.66	5.749[e], 5.70[f]	5.90[d]	63.47	57[e], 68.5[f]	72[d]

[a] Ref. [48].
[b] Ref. [49].
[c] Ref. [50].
[d] Ref. [51].
[e] Ref. [52].
[f] Ref. [53].

Table 2
Calculated zinc-blende (ZB) phase structural parameters for $ZnO_{1-x}Te_x$ alloys compared with experimental and other theoretical calculations.

Composition	Lattice constant a (Å)			Bulk modulus B (GPa)		
X	WC-GGA	Other calculations	Exp.	WC-GGA	Other calculations	Exp.
0	4.55	4.504[b], 4.614[c]	4.614[a]	158.92	160.8[b], 156.8[c]	156.8[a]
0.25	4.96			113.74		
0.50	5.36			79.45		
0.75	5.63			70.72		
1	6.04	6.158[e], 6.06[f]	6.1037[d]	45.88	47.5[e], 50.54[f]	51–52.8[d]

[a] Ref. [48].
[b] Ref. [49].
[c] Ref. [50].
[d] Ref. [51].
[e] Ref. [52].
[f] Ref. [53].

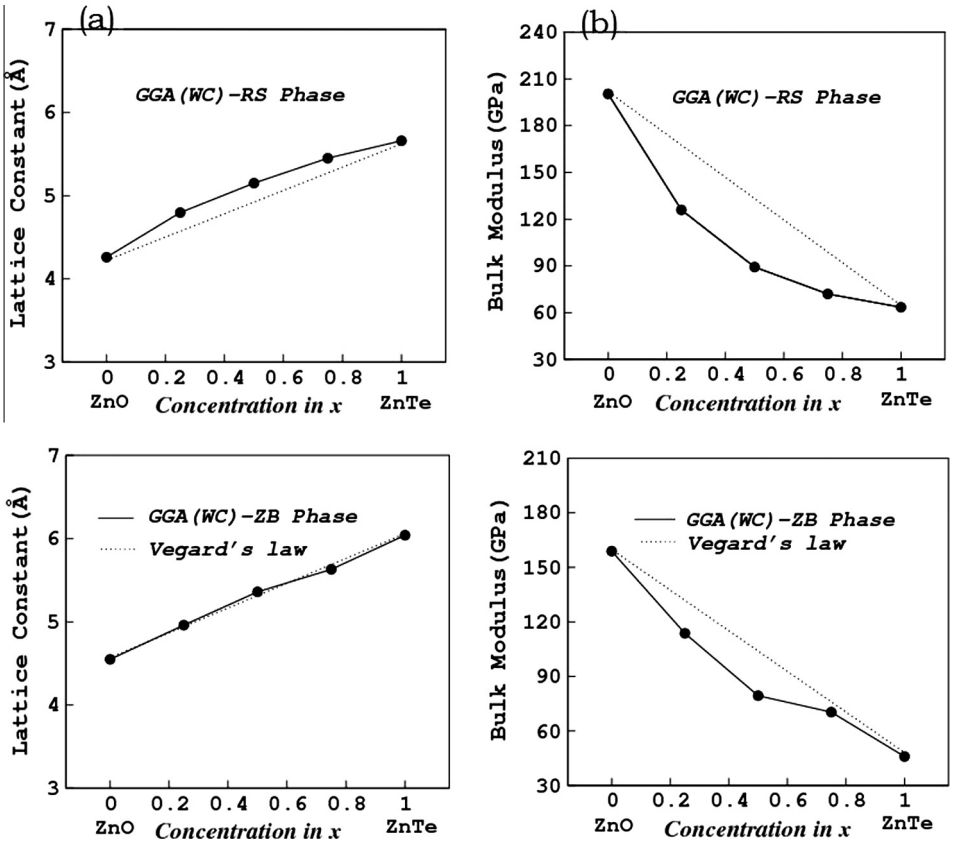

Fig. 3. Composition dependence of (a) lattice constant (left panel) and (b) bulk modulus (right panel) for $ZnO_{1-x}Te_x$ alloys in RS and ZB phases.

of end binary compounds and the differences in the electronic configuration of host lattice and dopant species yield structural properties that are divergent from Vegard's law which expects the variation of structural properties to be only dependent upon the structural parameters of end binary compounds.

3.2. Electronic properties

The functional application of materials in various electronic devices requires a thorough understanding of energy band gaps along with aligned conduction band valleys. For the RS and ZB phases, the electronic band structures of $ZnO_{1-x}Te_x$ alloys were computed using WC-GGA, EV-GGA and mBJLDA schemes. The band gap values, computed using the mBJLDA, for solids have a sound agreement with that of experimental data and this agreement is of the same order which can be achieved with computationally expensive GW or hybrid functional methods [40]. The electronic band structures obtained with mBJLDA for the studied compounds are shown in Fig. 4, while the band gap values computed by employing the WC-GGA, EV-GGA and mBJLDA are compared in Table 3.

In RS phase, the compounds under study appear to be metallic as valence band (VB) maximum and conduction band (CB) minimum meet at the Fermi level. Whereas, in ZB phase both the VB maximum and CB minimum reside at Γ-point of the Brillouin zone for all considered dopant concentrations. Referring to Table 3, the band gap values are higher in case of mBJLDA than those obtained using WC-GGA and EV-GGA signifying the improvement of electronic band structure as compared to the underestimations commonly observed for LDA and GGA calculations [40,41]. It is also worth mentioning here the effect of supercell size on the electronic properties of the compounds under study. As mentioned earlier,

Table 3
Zinc-blende (ZB) phase band gaps for $ZnO_{1-x}Te_x$ alloys along Γ–Γ symmetry points with WC-GGA, EV-GGA and mBJLDA functionals.

Composition	Band gap energy (eV)				
X	WC-GGA	EV-GGA	mBJLDA	Exp.	Other calculations
0	0.70	1.50	2.60	3.27[a]	0.86[a]
0.25	0.60	1.10	2.30		
0.50	0.40	0.80	1.10		
0.75	0.20	0.50	0.70		
1	1.20	1.90	2.40	2.38[b]	1.102[c]

[a] Ref. [54].
[b] Ref. [55].
[c] Ref. [53].

we have also performed band structure calculations using larger (32-atom) ZB supercells to see the effects originating from increasing the number of neighboring atoms and symmetry reduction on the electronic properties. We note, as expected due to reduction of crystallographic symmetry, that at high symmetry points (except at Γ-point) the band structure profiles for 8-atom and 32-atom cells show notable difference, however, the direct (Γ–Γ) band gaps computed using WC-GGA, EV-GGA and mBJLDA remain unchanged.

In order to have a deeper understanding of electronic structures of the studied compounds in RS and ZB phases, the total and partial density of states (DOS) have also been calculated. For all employed DFT approximations, the contribution to the total and partial DOS in VB and CB are almost similar and the results obtained with mBJLDA are shown in Fig. 5. In Fig. 5(a and b), the total DOS (TDOS) of $ZnO_{1-x}Te_x$ alloys at different x concentrations are depicted along with their partial DOS (PDOS) in which Zn-3d, O-2p and Te (5s, 5p) states are plotted. In ZB phase, both of end binaries (ZnO and ZnTe) have distinct energy band gaps (Fig. 5b), and it is noted that Zn-3d, O-2p and Te-5p states are dominant in making valence bands in these binaries whereas s states of Zn and Te form conduction band in ZnTe. In case of ternary alloys $ZnO_{1-x}Te_x$ (x = 0.25, 0.50 and 0.75), the bottom of valence band is totally dominated by Zn-3d and Te-5p states but the top and bottom of conduction band are occupied by Zn-4s and Te-5s states, respectively. Overall direct band gap semiconductor behavior is observed in all ZB ternary alloys $ZnO_{1-x}Te_x$.

3.3. Optical properties

In order to examine the optical response of compounds under study, it is conventional to take into account the transitions of electrons from occupied energy bands to unoccupied energy bands, particularly at high symmetry points in the Brillouin zone. Behavior of any physical system in the presence of external electromagnetic radiation is described by the dielectric function. Since this interaction primarily depends upon photons, their polarization plays a decisive role in the optical response. The complex dielectric

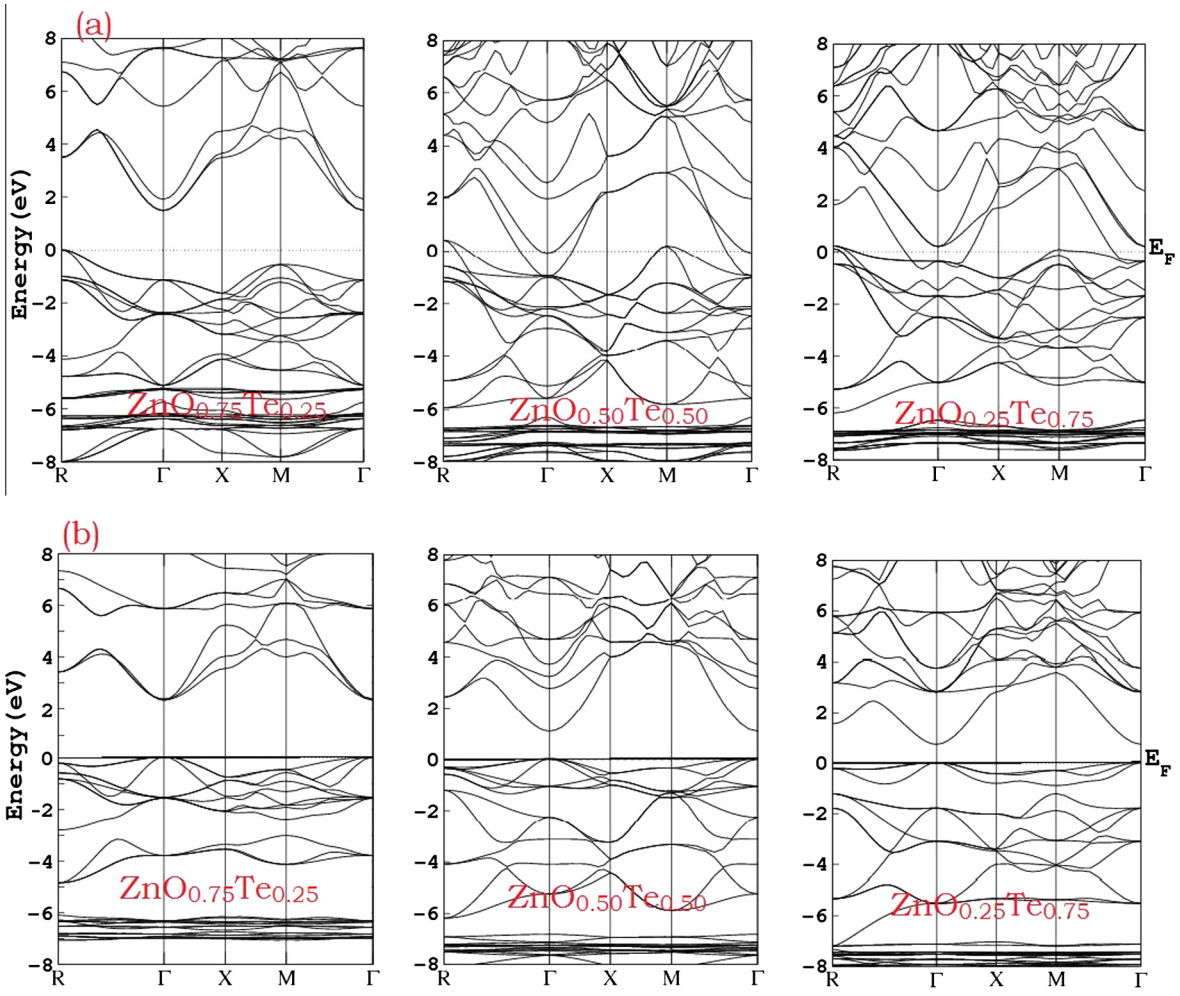

Fig. 4. Electronic band structures plot computed using the mBJLDA functional for $ZnO_{1-x}Te_x$ alloys at x = 0.25, 0.50 and 0.75 in (a) RS and (b) ZB phases.

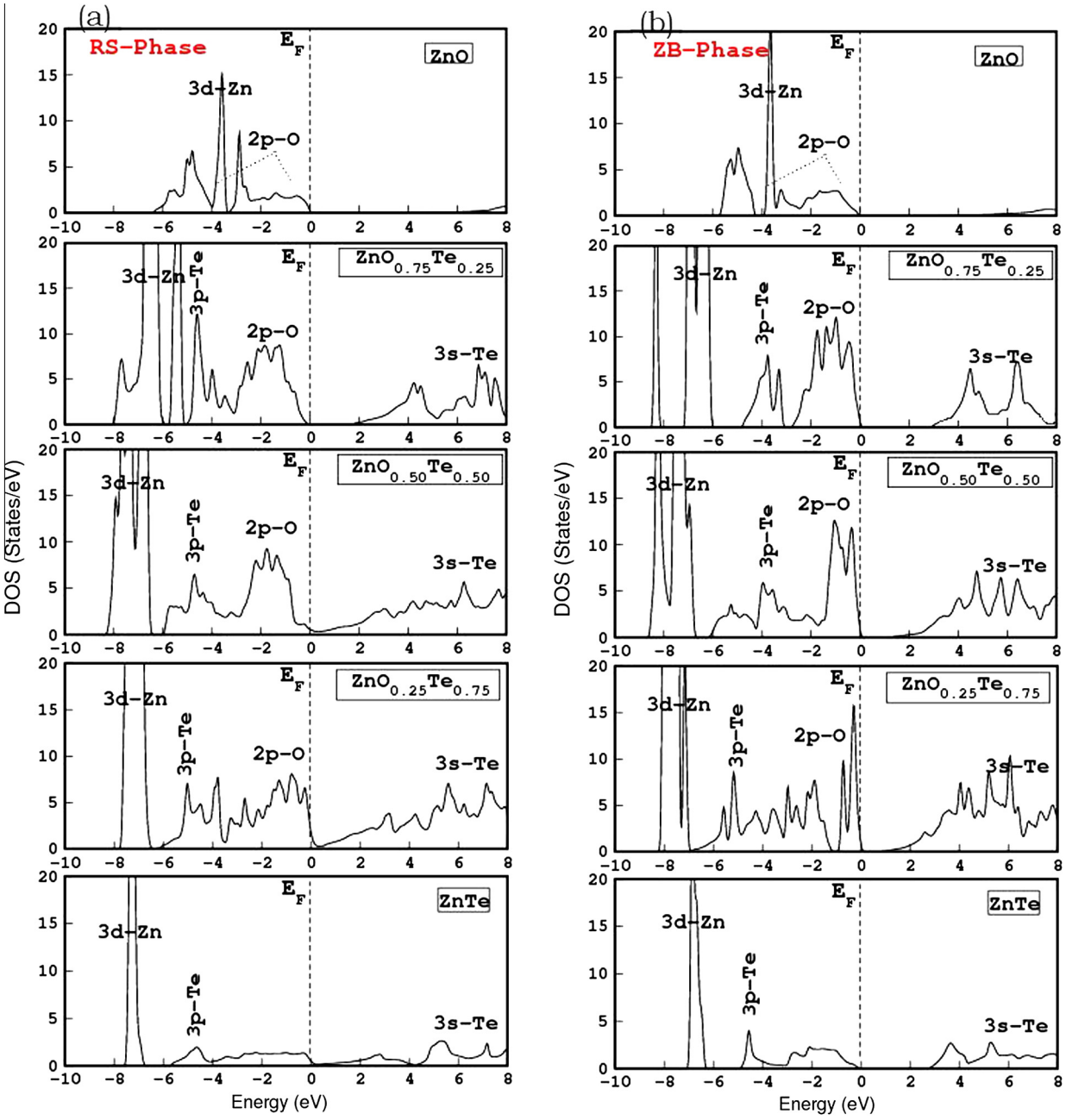

Fig. 5. Total along with partial density of states (DOS) computed using the mBJLDA functional for $ZnO_{1-x}Te_x$ alloys at $x = 0.0$, 0.25, 0.50, 0.75 and 1.0 in (a) RS and (b) ZB phases.

function $\varepsilon(\omega) = \varepsilon_{real}(\omega) - i\varepsilon_{imaginary}(\omega)$ is helpful to explore the optical properties of solids. The calculations for the electronic structures have been used to compute the imaginary part ($\varepsilon_{imaginary}(\omega)$), in long wavelength limit, by utilizing joint DOSs and the optical matrix elements [42]

$$\varepsilon_{imaginary}(\omega) = \frac{e^2 h}{\pi m^2 \omega^2} \sum \int \left[|M_{c,v}(k)|^2 \delta[\omega_{c,v}(k) - \omega] \right] d^3k \qquad (1)$$

where $M_{c,v}(k)$ indicate the moment dipole elements intending the direct transitions of electron between VB and CB states, and $\omega_{c,v}(k) = E_{ck} - E_{vk}$ are the transition energy. The imaginary part of the complex dielectric function can be used in the Kramers–Kronig relation to evaluate the real part [43].

Table 4
Zinc-blende (ZB) phase calculated optical parameters for $ZnO_{1-x}Te_x$alloys with mBJLDA functional.

x	E_g (eV)	$\varepsilon_1(0)$	$R(0)$	$n(0)$	Critical points values			
					ε_2	K	A	σ
$ZnO_{1-x}Te_x$								
0	2.60	3.14	0.07	1.72	1.54	0.94	2.08	1.69
0.25	2.30	5.29	0.14	2.26	0.71	0.71	1.04	1.12
0.50	1.10	5.35	0.16	2.37	2.13	2.13	2.78	2.44
0.75	0.70	7.16	0.20	2.64	0.94	1.30	1.56	1.50
1	2.40	8.56	0.23	2.88	1.15	1.06	1.73	1.30

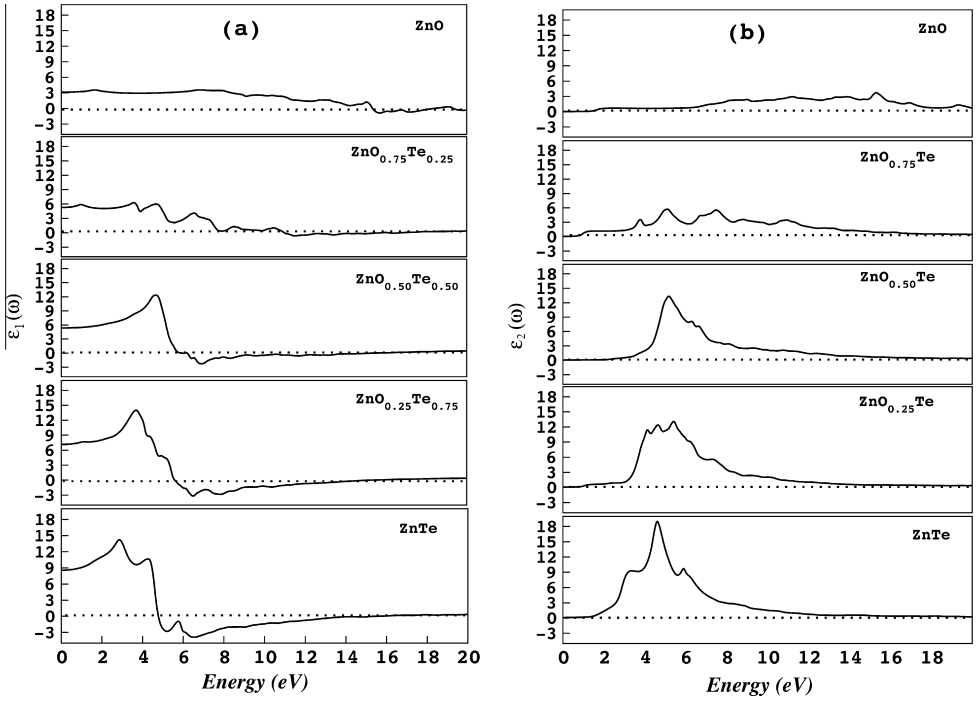

Fig. 6. The calculated (a) $\varepsilon_{real}(\omega)$ and (b) $\varepsilon_{imagnary}(\omega)$ parts of dielectric function for $ZnO_{1-x}Te_x$ alloys at $x = 0.0, 0.25, 0.50, 0.75$ and 1.0.

$$\varepsilon_{real}(\omega) = 1 + \chi + \frac{Ne^2}{\varepsilon_0 m_0} \frac{\omega_0^2 - \omega^2}{(\omega_0^2 - \omega^2)^2 + (\gamma\omega)^2} \quad (2)$$

The $\varepsilon_{real}(\omega)$ and $\varepsilon_{imagnary}(\omega)$ parts of the dielectric function are shown in Fig. 6(a and b), such that the former part corresponds to incident photons dispersion from the materials while the energy absorbed by these materials is represented by the latter. For our alloys system, the $\varepsilon_{imaginary}(\omega)$ parts at $0 \leqslant x \leqslant 1$ are plotted in Fig. 6(b) and their corresponding onset critical points are listed in Table 4. It is obvious from the obtained results that increasing Te concentration in ZnO makes the peaks sharp and shift them towards lower values of photon energy. For ZnO, $\varepsilon_{real}(\omega)$ is positive up to 15.30 eV and shows small peaks at 1.7 eV, 6.9 eV, 12.86 eV and 15.01 eV. Similarly, for ZnTe, it is positive up to 4.70 eV and has two peaked at 2.91 eV and 4.21 eV. For the ternaries, the $\varepsilon_{real}(\omega)$ has positive values up to 10.91 eV, 6.19 eV, 5.54 eV for $x = 0.25, 0.50, 0.75$, respectively. Two strong absorption regions are observed for $ZnO_{0.75}Te_{0.25}$ and ZnO in the energy ranges

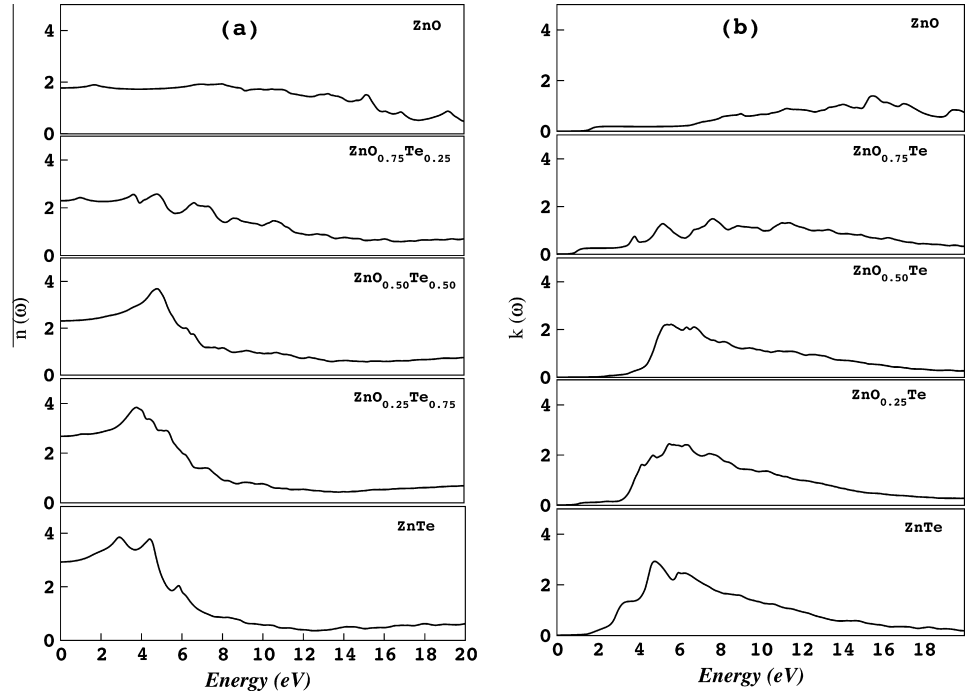

Fig. 7. The calculated (a) refractive index $n(\omega)$ and (b) extinction coefficient $k(\omega)$ for $ZnO_{1-x}Te_x$ alloys at $x = 0.0, 0.25, 0.50, 0.75$ and 1.0.

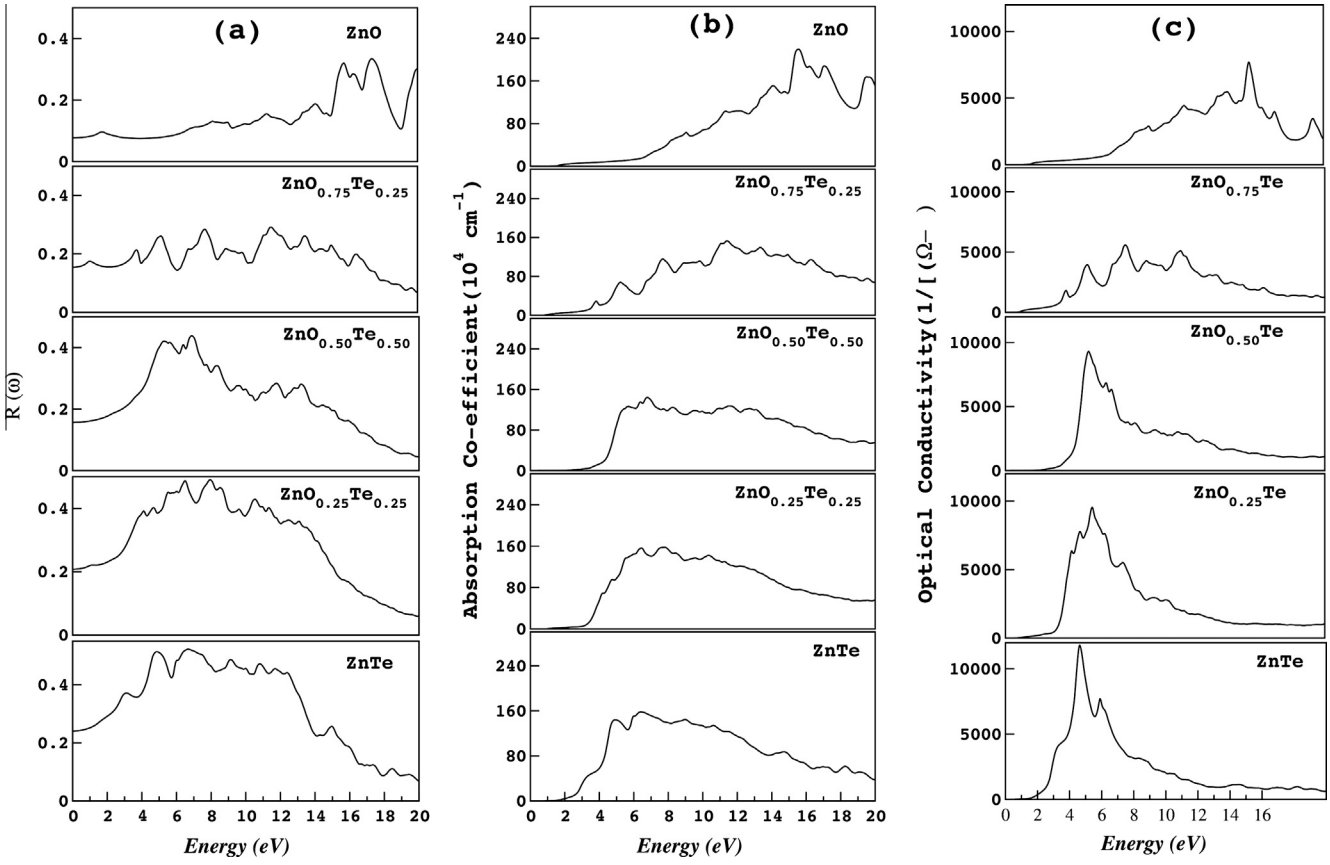

Fig. 8. The calculated (a) refractivity $R(\omega)$, (b) absorption coefficient $\alpha(\omega)$ and (c) optical conductivity $\sigma(\omega)$ for $ZnO_{1-x}Te_x$ alloys at $x = 0.0, 0.25, 0.50, 0.75$ and 1.0.

0.52–10.79 eV and 0.96–15.3 eV respectively. In these energy ranges, $\varepsilon_{real}(\omega)$ fluctuates between its maximum to minimum values such that the photon propagation takes places for $\varepsilon_{real}(\omega) > 0$, damping of electromagnetic wave for $\varepsilon_{real}(\omega) < 0$ and finally the longitudinally polarized waves originate for $\varepsilon_{real}(\omega) = 0$. Moreover, the zero frequency limit $\varepsilon_{real}(0)$ determines the dielectric response to the static electric field. Its values for the different concentrations are given in Table 4 and an increase/decrease is found in $\varepsilon_{real}(0)$/band gap while going from $x = 0$ to 1. It is to be noted that $\varepsilon_{real}(0)$ is energy band gap dependent and it is in accordance with the Penn Model [44] as:

$$\varepsilon_{real}(\omega) = 1 + \left(\frac{\hbar\omega_p}{E_g}\right)^2 \quad (3)$$

where E_g and ω_p are the energy band gap and plasma frequency, respectively. In above relation, if $\varepsilon_{real}(0)$ is known then E_g and ω_p can also be calculated. The values of plasma frequencies are provided in Table 4 where it can be seen that like the mBJLDA band gaps the plasma frequencies reduces on going from $x = 0$ to $x = 0.75$. The maximum value of ω_p is achieved for the binary ZnTe which is in confirmation with the nonlinear variation of mBJLDA band gap values presented in Table 3. In the obtained spectra, one of the peaks is present and it shifting towards the low energy region with the increasing values of x. With certain energy, the compounds illustrate metallic behavior when $\varepsilon_{real}(\omega)$ goes down the unity.

Refractive index measures the transparency of semiconductors against spectral radiations and has a key role in evaluating their optical and electronic properties. In addition to these properties, refractive index has essential impact for the devices such as wave guides, detectors and solar cell [45]. Mostly in semiconductors, empirical relations [46,47] relate refractive index and energy band gap, and these two quantities help in deriving many other optical properties. The refractive index of ternary alloys $ZnO_{1-x}Te_x$ within $0 \leqslant x \leqslant 1$ range are displayed in Fig. 7(a). For $ZnO_{0.50}Te_{0.50}$, static refractive index $n(0) = 2.37$. It is energy dependent and reaches the peak value at about 3.6288 eV in ultraviolet region and then reduces to the minimum value at 13.24 eV. Fig. 7(b) depicts the extinction coefficient $k(\omega)$ whose local maxima is closely related to the zero of $\varepsilon_{real}(\omega)$ (5.38 eV). From the Figs. 6(a) and 7(b), the real parts of DF and refractive index have close association with each other.

Referring to Figs. 6a and 7b, it is evident that the real parts of dielectric function and refractive index (i.e. $\varepsilon_1(\omega)$ and $n(\omega)$) have close relation with each other. The other calculated parameters for $ZnO_{1-x}Te_x$ alloy at all doping concentrations are refractivity $R(\omega)$, absorption coefficient $\alpha(\omega)$ and optical conductivity $\sigma(\omega)$. Their plots are shown in Fig. 8(a–c) and the values of corresponding critical points are presented in Table 4. The critical point values vary in accordance with the direct energy band gap values listed in Table 3.

4. Conclusions

Using first-principles calculations and considering special quasi-random structure (SQS) approach for RS and ZB phase, we evaluated the structural, electronic and optical properties of ternary alloys $ZnO_{1-x}Te_x$ within the range $0 \leqslant x \leqslant 1$. We have calculated the variation in lattice parameters, bulk modulus, energy band gap, dielectric function and refractive index with respect to the doping concentrations. It is found that the concentration dependent lattice parameter and bulk modulus significantly deviate from the Vegard's law. This deviation is due to the binary

compounds ZnO and ZnTe having significantly mismatched lattice parameters and bulk modulus. In addition to WC-GGA and EV-GGA, electronic properties have been computed by using more efficient mBJLDA functional of DFT and the results are found in good agreement with experimental results. ZB phase $ZnO_{1-x}Te_x$ have semiconducting direct band gap behavior, whereas indirect band gap are obtained for RS phase at concentrations $x = 0$ and 0.25. Finally, analysis of the frequency dependent complex dielectric function in terms of critical point structure yields the identification of the optical transitions in the alloys system under investigation.

Acknowledgement

For the author A.H. Reshak, the result was developed within the CENTEM Project, reg. No. CZ.1.05/2.1.00/03.0088, co-funded by the ERDF as part of the Ministry of Education, Youth and Sports OP RDI program. MetaCentrum and the CERIT-SC under the program Center CERIT Scientific Cloud reg. No. CZ.1.05/3.2.00/08.0144.

References

[1] D.C. Look, J. Electron Mater. 35 (2006) 1299.
[2] S.J. Pearton, D.P. Norton, K. Ip, Y.W. Heo, T. Steiner, Prog. Mater. Sci. 50 (2005) 293.
[3] U. Ozgur, Y.I. Alivov, C. Liu, A. Teke, M.A. Reshchikov, J. Appl. Phys. 98 (2005) 041301.
[4] S. Dutta, S. Chattopadhyay, A. Sarkar, M. Chakrabarti, D. Sanyal, D. Jana, Prog. Mater. Sci. 54 (2009) 89.
[5] K.M. Wong, S.M. Alay-e-Abbas, Y. Fang, A. Shaukat, Y. Lei, J. Appl. Phys. 114 (2013) 034901.
[6] K.M. Wong, S.M. Alay-e-Abbas, A. Shaukat, Y. Fang, Y. Lei, J. Appl. Phys. 113 (2013) 014304.
[7] Y. Lv, W. Xiao, W. Li, J. Xue, J. Ding, Nanotechnology 24 (2013) 175702.
[8] D.C. Look, Mater. Sci. Eng. B 80 (2001) 383.
[9] U. Rau, M. Schmidt, Thin Solid Films 387 (2001) 141.
[10] S. Itoh, S. Taniguchi, T. Hino, R. Imoto, K. Nakano, N. Nakayama, M. Ikeda, A. Ishibashi, Mater. Sci. Eng. B 43 (1997) 55.
[11] C. Klingshirn, Phys. Stat. Solidi (b) 244 (2007) 3027.
[12] A. Sundaresan, R. Bhargavi, N. Rangarajan, U. Siddesh, C.N.R. Rao, Phys. Rev. B 74 (2006) 161306(R).
[13] H. Cao, Y.G. Zhao, S.T. Ho, E.W. Seelig, Q.H. Wang, R.P.H. Chang, Phys. Rev. Lett. 82 (1999) 2278.
[14] J. Xu, Q. Pan, Y. Shun, Z. Tian, Sens. Actuator B 666 (2000) 277.
[15] D.C. Look, D.C. Reynolds, J.R. Sizelove, R.L. Jones, C.W. Litton, G. Cantwell, W.C. Harsch, Solid State Commun. 105 (1998) 399.
[16] R.K. Thareja, A. Mitra, Appl. Phys. B 71 (2000) 181.
[17] H.D. Li, S.F. Yu, S.P. Lau, E.S.P. Leong, Appl. Phys. Lett. 89 (2006) 021110.
[18] H.C. Ong, J.Y. Dai, A.S.K. Li, G.T. Du, R.P.H. Chang, S.T. Ho, J. Appl. Phys. 90 (2001) 1663.
[19] J.V. Foreman, H.O. Everitt, J. Yang, J. Liu, Appl. Phys. Lett. 91 (2007) 011902.
[20] Q. Xu, H. Schmidt, S. Zhou, K. Potzger, M. Helm, H. Hochmuth, M. Lorenz, A. Setzer, P. Esquinazi, C. Meinecke, M. Grundmann, Appl. Phys. Lett. 92 (2008) 082508.
[21] J. Gu, K. Tonomura, N. Yoshikawa, J. Appl. Phys. 44 (1973) 4692.
[22] C. Winnewiser, P.U. Jensen, M. Schall, V. Schiyja, H. Helm, Appl. Phys. Lett. 70 (1997) 3069.
[23] J.M. Pawlikoswski, Thin solid Films 127 (1985) 39.
[24] K.U. Raju, RP. Vijalayakshmi, R. Venugopal, D.R. Reddy, B. Reddy, Mater. Lett. 13 (1992) 336.
[25] M.H.R. Khan, J. Phys. D: Appl. Phys. 27 (1994) 2190.
[26] W.I. Tao, M. Jurkovice, I.W. Wang, Appl. Phys. Lett. 64 (1994) 1848.
[27] N.B. Chaure, R. Jayakrishnan, J.P. Nair, R.K. Pandey, Semicond. Sci. Technol. 12 (1997) 1171.
[28] X.F. Fan, Z.X. Shen, Y.M. Lu, J.L. Kuo, New J. Phys. 11 (2009) 093008.
[29] A. Zunger, S.-H. Wei, L.G. Feireira, J.E. Bernard, Phys. Rev. Lett. 65 (1990) 353.
[30] C. Jiang, C. Wolverton, J. Sofo, L.-Q. Chen, Z.-K. Liu, Phys. Rev. B 69 (2004) 214202.
[31] P. Blaha, K. Schwarz, G.K.H. Madsen, D. Hvasnicka, J. Luitz, WIEN2k, An Augmented Plane Wave + Local Orbitals Program for Calculating Crystal Properties, Karlheinz Schwarz, Techn. Universit Wien, Austria, 2001.
[32] Z. Wu, R.E. Cohen, Phys. Rev. B 73 (2006) 235116.
[33] N.A. Noor, N. Ikram, S. Ali, S. Nazir, S.M. Alay-e-Abbas, A. Shaukat, J. Alloys Compd. 507 (2010) 356.
[34] E. Engel, S.H. Vosko, Phys Rev. B 47 (1991) 13164.
[35] F. Tran, P. Blaha, Phys. Rev. Lett. 102 (2009) 226401.
[36] B.K. Agrawal, S. Agrawal, P.S. Yadav, S. Kumar, J. Phys.: Condens. Matter 9 (1997) 1763.
[37] J.S. Almeida, R. Ahuja, Appl. Phys. Lett. 89 (2006) 061913.
[38] N.A. Noor, W. Tahir, Fatima Aslam, A. Shaukat, Physica B 407 (2012) 943.
[39] L. Vegard, Z. Phys. 5 (1921) 17.
[40] D.J. Singh, Phys. Rev. B 82 (2010) 205102.
[41] F. Tran, P. Blaha, K. Schwarz, J. Phys. Condens. Matter 19 (2007) 196208.
[42] C. Ambrosch-Draxl, J.O. Sofo, Comput. Phys. Commun. 175 (2006) 1.
[43] F. Wooten, Optical Properties of Solids, Academic Press, New York, 1972.
[44] D.R. Penn, Phys. Rev. 128 (1962) 2093.
[45] N.M. Ravindra, P. Ganapathy, J. Choi, Infrared Phys. Technol. 50 (2007) 21.
[46] V.P. Gupta, N.M. Ravindra, Phys. Stat. Sol. B 10 (1980) 715.
[47] N.M. Ravindra, S. Auluck, V.K. Srivastava, Phys. Stat. Sol. B 93 (2003) 155.
[48] S. Desgreniers, Phys. Rev. B 58 (1998) 14102.
[49] J. Serrano, A.H. Romero, F.J. Manjoin, R. Lauck, M. Cardona, A. Rubio, Phys. Rev. B 69 (2004) 094306.
[50] J.E. Jaffe, A.C. Hess, Phys. Rev. B 48 (1993) 7903.
[51] Numerical Data and Functional Relationship in Science and Technology, Crystal and Solid State Physics, vol. 22, Springer, Berlin, 1984, Landolt-Bornstein New series Group III, vol. 22, Pts, Springer, Berlin, 1987.
[52] R. Franco, P. Mori-Sanchez, J.M. Recio, Phys. Rev. B 68 (2003) 195208.
[53] M. Lidner, G.F. Schlz, P. Link, H.P. Wagner, W. Kuhn, W. Gebhardt, J. Phys. Condens. Matter 4 (1992) 6401.
[54] H. Dixit, R. Saniz, D. Lamoen, B. Partoens, J. Comput. Phys. Commun. 182 (2011) 2029.
[55] N.E. Christensen, O.B. Christensen, Phys. Rev. B 33 (1986) 4739.